

Projected d-wave superconducting state: a fermionic projected entangled pair state study

Qi Yang,^{1,2} Xing-Yu Zhang,^{1,2} Hai-Jun Liao,^{1,3,*} Hong-Hao Tu,^{4,†} and Lei Wang^{1,3,‡}

¹*Institute of Physics, Chinese Academy of Sciences, Beijing 100190, China*

²*University of Chinese Academy of Sciences, Beijing 100049, China*

³*Songshan Lake Materials Laboratory, Dongguan, Guangdong 523808, China*

⁴*Institute of Theoretical Physics, Technische Universität Dresden, 01062 Dresden, Germany*

(Dated: August 10, 2022)

We investigate the physics of projected d-wave pairing states using their fermionic projected entangled pair state (fPEPS) representation. First, we approximate a d-wave Bardeen–Cooper–Schrieffer state using the Gaussian fPEPS. Next, we translate the resulting state into fPEPS tensors and implement the Gutzwiller projection which removes double occupancy by modifying the local tensor elements. The tensor network representation of the projected d-wave pairing state allows us to evaluate physical quantities in the thermodynamic limit without employing the Gutzwiller approximation. Despite having very few variational parameters, such physically motivated tensor network states are shown to exhibit competitive energies for the doped t - J model. We expect that such construction offers useful initial states and guidance for variational tensor network calculations.

I. INTRODUCTION

The projected Bardeen–Cooper–Schrieffer (BCS) states play a prominent role in the studies of strongly correlated electrons [1]. The state is obtained by eliminating the double occupancies in the BCS wave function

$$|\Psi\rangle = P_G|\text{BCS}\rangle, \quad (1)$$

where $P_G = \prod_i (1 - n_{i\uparrow}n_{i\downarrow})$ is the Gutzwiller projection operator which implements the projection. The state consists of resonating valence bonds (RVBs), which are believed to be relevant to superconducting cuprates [2–4], frustrated magnets [5], and a broad range of other phenomena in strongly correlated physics. Subsequent theoretical and numerical investigations show that the projected BCS state in Eq. (1) is indeed the low-energy candidate state of the relevant t - J models and exhibits similar features as observed in superconducting cuprates [6–11].

To account for further intricacies such as competing orders, the vanilla RVB state [4] has developed into a full-fledged variational wave function [12–16]. Along with developments of other numerical methods [17–24], a point has been reached where uncertainties in the model Hamiltonian are even larger than the achieved accuracy of a many-body solver. The situation calls for more realistic models with inputs from ab initio calculations and experiments. In the meantime, it is worth pursuing deeper synergy between different methods beyond simply cross-checking their numerical data [18]. Such synergy will bridge the worlds of “educated guess of wave functions” and “solving Hamiltonians numerically”, potentially offering more physical understandings.

An example of such promising synergy is to cast the family of projected BCS states into tensor network states. Recently, a number of works develop methods for converting projected fermionic states into matrix product states [25–34] and use

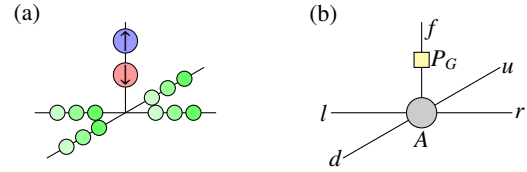


FIG. 1. (a) The local fiducial state in Eq. (5) of a fPEPS. It is a state formed by the physical fermions of spin up and down (blue and red dots) and Λ flavors of virtual fermions reside on the bond (green dots). The state is fully characterized by the local correlation matrix in Eq. (6) if it is Gaussian. (b) Gutzwiller projection to the local fPEPS tensor.

such translation to inspect state fidelity, study their entanglement properties, and facilitate density-matrix renormalization group calculations.

Extending this progress to convert projected fermionic states into two-dimensional tensor networks is highly desirable as this will allow one to investigate projected BCS states using methods from the tensor network toolbox. Along this line, there have been works constructing tensor network representations of the RVB states based on their real space picture [35–37]. In this work, we present a more systematic approach to achieve the translation and use it to investigate the projected d-wave pairing state in an infinite two-dimensional lattice.

Our starting point is a fermionic quadratic Hamiltonian with d-wave pairing on the square lattice,

$$H_{\text{BCS}} = \sum_{\mathbf{k},\sigma} \xi_{\mathbf{k}} f_{\mathbf{k}\sigma}^\dagger f_{\mathbf{k}\sigma} + \sum_{\mathbf{k}} \left(\Delta_{\mathbf{k}} f_{\mathbf{k}\uparrow}^\dagger f_{-\mathbf{k}\downarrow}^\dagger + \Delta_{\mathbf{k}}^* f_{-\mathbf{k}\downarrow} f_{\mathbf{k}\uparrow} \right), \quad (2)$$

where $f_{\mathbf{k}\sigma}$ ($f_{\mathbf{k}\sigma}^\dagger$) is the fermion annihilation (creation) operator in momentum space with spin index $\sigma = \uparrow, \downarrow$, $\xi_{\mathbf{k}} = -2t(\cos k_x + \cos k_y) - \mu$ and $\Delta_{\mathbf{k}} = 2\Delta_d(\cos k_x - \cos k_y)$. The hopping amplitude t is set to unity. The state $|\text{BCS}\rangle$ is the ground state of H_{BCS} parametrized by the chemical potential μ and the d-wave pairing amplitude Δ_d .

Given the BCS Hamiltonian in Eq. (2), we first find a Gaussian fermionic projected entangled pair state (fPEPS) [38] approximation to the pairing state $|\text{BCS}\rangle$ via a variational calcu-

* navyphysics@iphy.ac.cn

† hong-hao.tu@tu-dresden.de

‡ wanglei@iphy.ac.cn

lation. As shown in Fig. 1(a), the Gaussian fPEPS is formed by the physical fermions of spin up and down (blue and red dots) and Λ flavors of virtual fermions residing on each bond (green dots). Next, we translate the Gaussian fPEPS, parametrized by its correlation matrix, to fPEPS tensors and implement the Gutzwiller projection by locally modifying the tensor elements. Having an approximated fPEPS representation of the projected BCS state in Eq. (1) allows us to investigate its properties using tensor network algorithms. We examine the validity of the Gutzwiller approximation for the hole fugacity and report on the pairing order parameter and variational energy of the projected d-wave pairing state for the t - J model with various dopings.

II. METHOD

In this section, we present our method for obtaining the fPEPS tensors of a projected BCS state. We first review the construction of Gaussian fPEPS in Sec. II A with an emphasis on its connection to fPEPS. Subsequent steps follow the workflow in Figure 2.

A. Construction of Gaussian fPEPS

The fPEPS is formed by mediating the entanglement of physical fermions (f) on lattice sites via virtual fermions (u, l, d, r) residing on the bonds. Formally, it can be expressed as [38, 39]

$$|\Psi\rangle = \left[\bigotimes_{\langle \mathbf{i}, \mathbf{j} \rangle} \langle \omega_{\mathbf{ij}} | \right] \left[\bigotimes_{\mathbf{i}} |A_{\mathbf{i}}\rangle \right], \quad (3)$$

where $|\omega_{\mathbf{ij}}\rangle$ is a maximally entangled state of virtual fermions on the $\langle \mathbf{i}, \mathbf{j} \rangle$ bond. More concretely, we use $u_{i\alpha}, l_{i\alpha}, d_{i\alpha}, r_{i\alpha}$ to denote the annihilation operators of the virtual fermions at site \mathbf{i} , where $\alpha \in [1, \dots, \Lambda]$ is the flavor index and u, l, d, r refer to up, left, down, and right, respectively. The horizontal bond between two neighboring sites \mathbf{i} and $\mathbf{j} = \mathbf{i} + \hat{\mathbf{x}}$ is defined by

$$|\omega_{\mathbf{ij}}\rangle = \prod_{\alpha=1}^{\Lambda} \frac{1}{\sqrt{2}} (1 + r_{i\alpha}^\dagger l_{j\alpha}^\dagger) |\text{vac}\rangle, \quad (4)$$

where $|\text{vac}\rangle$ is the vacuum of virtual fermions. The vertical bonds are defined in a similar way.

Next, the local fiducial state is generally expressed as

$$|A_{\mathbf{i}}\rangle = \sum_{f,u,l,d,r} A_{uldr}^f |f\rangle \otimes |uldr\rangle, \quad (5)$$

where $|f\rangle$ denotes the local physical states, consisting of empty, singly occupied (with either spin up or down), and doubly occupied states. The basis $|uldr\rangle$ corresponds to the Fock space of virtual fermions at site \mathbf{i} .

Since the virtual bonds are fermionic Gaussian states, the fPEPS in Eq. (3) would also be Gaussian, as long as the local fiducial state in Eq. (5) is a fermionic Gaussian state.

Such a state forms a subclass of fPEPS, namely the Gaussian fPEPS [38]. The flavor number of virtual fermions controls the expressibility of the Gaussian fPEPS. In the usual fPEPS language, a Gaussian fPEPS with Λ virtual fermion residing on the bonds between neighboring sites has a bond dimension $D = 2^\Lambda$.

A great computational advantage of the Gaussian fPEPS is that a powerful fermionic Gaussian formalism [40] can be used for performing efficient computations, which we briefly outline below. Throughout this work we consider translationally invariant fPEPS with a one-site unit cell (generalization to multi-site unit cells is straightforward though) and omit the site index of the fiducial state. Let us label the physical and virtual fermions at a local site as $(c_1, c_2, c_3, \dots, c_{4\Lambda+2}) = (f_\uparrow, f_\downarrow, r_1, l_1, r_2, l_2, \dots, r_\Lambda, l_\Lambda, d_1, u_1, d_2, u_2, \dots, d_\Lambda, u_\Lambda)$. In terms of Majorana operators $\gamma_{2\mu-1} = c_\mu^\dagger + c_\mu$ and $\gamma_{2\mu} = -i(c_\mu^\dagger - c_\mu)$, the local fiducial state (5), being a fermionic Gaussian state, is fully characterized by its correlation matrix

$$\Gamma_{\mu\nu} = \frac{i}{2} \langle A | [\gamma_\mu, \gamma_\nu] | A \rangle, \quad (6)$$

where Γ is a real antisymmetric matrix satisfying $\Gamma^2 = -\mathbb{I}_{(8\Lambda+4) \times (8\Lambda+4)}$. To proceed, the correlation matrix (6) is parametrized as

$$\Gamma = \begin{pmatrix} A & B \\ -B^T & D \end{pmatrix} \quad (7)$$

with A, B, D being 4×4 , $4 \times 8\Lambda$, and $8\Lambda \times 8\Lambda$ matrices, respectively.

In the translationally invariant setup, both virtual and physical Majorana modes can be transformed into modes in momentum space with $\gamma_{\mathbf{k},\mu} = \frac{1}{\sqrt{N}} \sum_{\mathbf{j}} \exp(-i\mathbf{k} \cdot \mathbf{j}) \gamma_{\mathbf{j},\mu}$ where N is the number of sites. The allowed values of \mathbf{k} satisfy $\mathbf{k} = \frac{2\pi\mathbf{n}}{L}$ where $\mathbf{n} \in \mathbb{Z} \oplus (\mathbb{Z} + \frac{1}{2})$ if the system has periodic (antiperiodic) boundary condition along \mathbf{x} (\mathbf{y}) direction [41]. Denoting the virtual bonds as $|\omega\rangle$, the correlation matrix of the virtual bonds is written as $(G_{\mathbf{k}}^\omega)_{\mu\nu} = \frac{i}{2} \langle \omega | [\gamma_{\mathbf{k},\mu}, \gamma_{-\mathbf{k},\nu}] | \omega \rangle$ ($\mu, \nu = 5, \dots, 8\Lambda + 4$) and takes the following explicit form:

$$G_{\mathbf{k}}^\omega = \bigoplus_{\mu=1}^{\Lambda} \left[\begin{pmatrix} e^{ik_x} \mathbb{I}_{2 \times 2} \\ -e^{-ik_x} \mathbb{I}_{2 \times 2} \end{pmatrix} \oplus \begin{pmatrix} e^{iky} \mathbb{I}_{2 \times 2} \\ -e^{-iky} \mathbb{I}_{2 \times 2} \end{pmatrix} \right]. \quad (8)$$

The correlation matrix of the Gaussian fPEPS (3), defined by

$$(G_{\mathbf{k}}^f)_{\mu\nu} = \frac{i}{2} \langle \Psi | [\gamma_{\mathbf{k},\mu}, \gamma_{-\mathbf{k},\nu}] | \Psi \rangle, \quad (\mu, \nu = 1, \dots, 4), \quad (9)$$

is calculated by contracting the virtual modes and gives rise to

$$G_{\mathbf{k}}^f = A + B(D + G_{\mathbf{k}}^\omega)^{-1} B^T. \quad (10)$$

This is a key result for the variational calculation below. The proof of Eq. (10) is given in Appendix A.

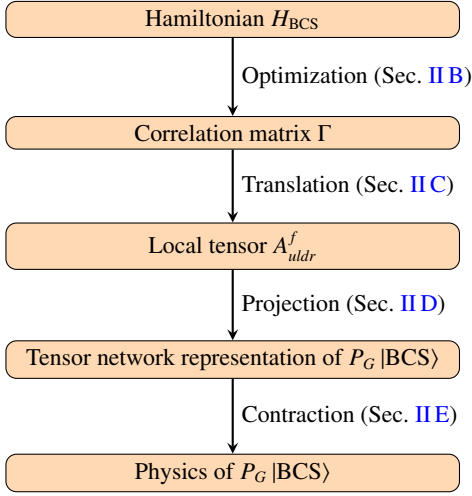


FIG. 2. The recipe for preparing a Gutzwiller projected BCS state in Eq. (1) as a fermionic PEPS and investigating its physical properties via tensor network contraction.

B. Variational optimization of Gaussian fPEPS

For the next step, we determine an optimal Gaussian fiducial state (5), such that the variational energy of the Hamiltonian H_{BCS} [see Eq. (2)] is minimized within the family of Gaussian fPEPS for a given flavor number Λ . The BCS ground state of H_{BCS} is thus approximated by a Gaussian fPEPS. By using the correlation matrix in Eq. (9), the variational energy can be expressed as

$$\langle H_{\text{BCS}} \rangle = \sum_{\mathbf{k}} \xi_{\mathbf{k}} (\rho_{\mathbf{k}\uparrow} + \rho_{\mathbf{k}\downarrow}) + \Delta_{\mathbf{k}} \eta_{\mathbf{k}} + \Delta_{\mathbf{k}}^* \eta_{\mathbf{k}}^* \quad (11)$$

with $\rho_{\mathbf{k}\sigma} = \langle f_{\mathbf{k}\sigma}^\dagger f_{\mathbf{k}\sigma} \rangle$ and $\eta_{\mathbf{k}} = \langle f_{\mathbf{k}\uparrow}^\dagger f_{-\mathbf{k}\downarrow}^\dagger \rangle$, which can be evaluated via the relation $\sum_{\mathbf{k}} \xi_{\mathbf{k}} \langle f_{\mathbf{k}\uparrow}^\dagger f_{\mathbf{k}\uparrow} \rangle = \sum_{\mathbf{k}} \xi_{\mathbf{k}} [\frac{1}{2} - \frac{1}{2}(G_{\mathbf{k}}^f)_{1,2}]$, $\sum_{\mathbf{k}} \xi_{\mathbf{k}} \langle f_{\mathbf{k}\downarrow}^\dagger f_{\mathbf{k}\downarrow} \rangle = \sum_{\mathbf{k}} \xi_{\mathbf{k}} [\frac{1}{2} - \frac{1}{2}(G_{\mathbf{k}}^f)_{3,4}]$ and $\eta_{\mathbf{k}} = \langle f_{\mathbf{k}\uparrow}^\dagger f_{-\mathbf{k}\downarrow}^\dagger \rangle = \frac{1}{4} [(G_{\mathbf{k}}^f)_{1,4} + (G_{\mathbf{k}}^f)_{2,3} + i(G_{\mathbf{k}}^f)_{2,4} - i(G_{\mathbf{k}}^f)_{1,3}]$.

We carry out the optimization following Ref. [42]. The minimization is performed through the fiducial state's correlation matrix Γ in Eq. (7), which can be brought into a canonical form

$$\Gamma = X^T \left[\bigoplus_{\eta=1}^{4\Lambda+2} \begin{pmatrix} 0 & 1 \\ -1 & 0 \end{pmatrix} \right] X, \quad (12)$$

where X is an orthogonal matrix. The matrices A, B, D in Eq. (7) are hence functions of X , and so are the correlation matrix $G_{\mathbf{k}}^f$ in Eq. (10) and the variational energy in Eq. (11).

We optimize the real orthogonal matrix X by minimizing the loss function using optimization on the Stiefel manifold. The derivatives are calculated by using automatic differentiation with JAX [43]. The optimization algorithm is the conjugate gradient method offered by pymanopt [44]. This calculation was done for a finite lattice in the momentum space. Since the computational complexity scales linearly with the

system size, one can reach pretty large systems easily [42]. The accuracy of such variational calculation can be verified by comparing the results with the exact solution of the BCS Hamiltonian.

C. Translation of correlation matrix Γ into local tensor

To obtain the local tensor of Gaussian fPEPS $A_{uldr}^f = \langle f | \otimes \langle uldr | A_i \rangle$, we need to find out the fiducial state $|A_i\rangle$ based on its correlation matrix Γ .

To this end, we simply construct a single-site fiducial Hamiltonian

$$h = - \sum_{\mu\nu} i \Gamma_{\mu\nu} \gamma_\mu \gamma_\nu \quad (13)$$

using the correlation matrix for the fiducial state. This Hamiltonian is quadratic and contains $8\Lambda + 4$ types of Majorana fermions.

It is easy to prove that $|A_i\rangle$ is the unique ground state of the fiducial Hamiltonian h . By using the orthogonal matrix defined in Eq. (12), the Majorana operators can be rotated into a new basis as $\gamma' = X\gamma$. Notice that $(X\Gamma X^T)_{\mu\nu} = \frac{i}{2} \langle A_i | [\gamma'_\mu, \gamma'_\nu] | A_i \rangle = \left[\bigoplus_{\eta=1}^{4\Lambda+2} \begin{pmatrix} 0 & 1 \\ -1 & 0 \end{pmatrix} \right]_{\mu\nu}$, which shows that the Gaussian fiducial state $|A_i\rangle$ satisfies $i\gamma'_{2m-1}\gamma'_{2m} |A_i\rangle = |A_i\rangle$ ($m \in \mathbb{Z}$). As $i\gamma'_{2m-1}\gamma'_{2m}$ is a fermion parity operator and has eigenvalue ± 1 , the fiducial Hamiltonian $h = -i \sum_m \gamma'_{2m-1} \gamma'_{2m} = - \sum_{\mu\nu} i \Gamma_{\mu\nu} \gamma_\mu \gamma_\nu$ has $|A_i\rangle$ as its unique ground state.

We convert the fiducial Hamiltonian h from the Majorana basis to the original complex fermion basis [see Eq. (5)] and find its ground state by diagonalizing h . By reshaping the state vector $\in \mathbb{C}^{2^{4\Lambda+2}}$ into a five-leg tensor, we obtain A_{uldr}^f up to an unimportant overall phase.

Since the quadratic Hamiltonian conserves the fermion parity, its ground state $|A_i\rangle$ has a definite parity. Therefore, the tensor A_{uldr}^f automatically inherits \mathbb{Z}_2 symmetry as the parity of the state $|A_i\rangle$.

For obtaining the explicit form of $|A_i\rangle$, an exact diagonalization of the fiducial Hamiltonian h is manageable when the number of physical and virtual modes at each site is relatively small. This is indeed the case for our benchmark example, which already shows good performance. When the number of modes at each site is large, we provide a more efficient approach based on the state overlap in Appendix B.

D. Gutzwiller projection of Gaussian fPEPS

After obtaining a tensor network representation of the BCS state, we implement the Gutzwiller projection on the physical leg of the local tensor A_{uldr}^f as shown in Fig. 1(b). Since we carry out Gutzwiller projection in an infinite system in the grand canonical ensemble, we include a fugacity term in the empty configuration to account for the change of the particle density caused by the projection of double occupancies [45–48]. In this way, the projection operator reads $P_G =$

$\prod_{\mathbf{i}} z^{(1-n_{\uparrow}-n_{\downarrow})/2} (1 - n_{\uparrow}n_{\downarrow})$, where z is the fugacity of holes. The Gutzwiller projection operator is a local gate acting on the physical leg with the matrix representation: $\text{diag}(\sqrt{z}, 1, 1, 0)$ where the basis of this representation is $(|0\rangle, |\uparrow\rangle, |\downarrow\rangle, |\uparrow\downarrow\rangle)$. The zero in the Gutzwiller projection gate sets the local tensor elements associated with doubly occupied configurations to zero.

In principle, in a grand canonical calculation, one needs to tune the hole fugacity to maintain the average particle number. The Gutzwiller approximation [46] provides an estimation of the fugacity

$$z = \frac{2\delta}{1 + \delta}, \quad (14)$$

where δ is the hole density. One sees that in the undoped case, $\delta = 0$, the projection removes both empty and double occupancy configurations and only keeps singly occupied sites.

E. Tensor network contraction

The state after the Gutzwiller projection is no longer a Gaussian state. To investigate its physical properties, we employ tensor network contraction algorithms for fPEPS [49]. Since the optimization in Sec. II B can be done on a sufficiently large lattice, it is essentially free of finite-size error. Thus, after translation and Gutzwiller projection, we assemble the local tensors into an infinite lattice and employ infinite tensor network contraction algorithms. Note that one needs to take care of the swap gate [50] when contracting the local tensor since it is a fermionic tensor network.

To make the local tensor fully compatible with the diagrammatic notation for fPEPS in Ref. [49], one should pay special attention to the fermion sign associated with the order and form of virtual fermions in the definition of $|A_{\mathbf{i}}\rangle$ and $|\omega_{\mathbf{ij}}\rangle$.

For example, we need to make sure that the order of fermionic operators in the definition of $|A_{\mathbf{i}}\rangle$ in Gaussian fPEPS and fPEPS are the same. In Ref. [49], the ordering of fermions in the local tensor is $|ulfd\rangle$, while the tensor we obtained in Sec. II C follows the order $(c_1, c_2, \dots, c_{4\Lambda+2}) = (f_{\uparrow}, f_{\downarrow}, r_1, l_1, r_2, l_2, \dots, r_{\Lambda}, l_{\Lambda}, d_1, u_1, d_2, u_2, \dots, d_{\Lambda}, u_{\Lambda})$. In order to account for this difference, we introduce swap gates to transform between these two different orderings.

Additionally, in Ref. [49] it is free to contract the virtual bonds of two nearby fPEPS tensors without generating swap gates. This implies that the adopted definition of virtual fermion maximally entangled state is defined differently from Eq. (4). For example, for the bond between site \mathbf{i} and $\mathbf{j} = \mathbf{i} + \hat{\mathbf{x}}$, one has

$$|\omega_{\mathbf{ij}}^C\rangle = \frac{1}{\sqrt{2^\Lambda}} \sum_{\{n_\alpha\}} \prod_{\alpha=1}^{\Lambda} (r_{\mathbf{i}\alpha}^\dagger)^{n_\alpha} \prod_{\alpha=1}^{\Lambda} (l_{\mathbf{j}\alpha}^\dagger)^{n_\alpha} |\text{vac}\rangle, \quad (15)$$

where $n_\alpha \in \{0, 1\}$ is the occupation number of virtual fermions.

This differs from Eq. (4) by the ordering of virtual fermions if the number of flavors $\Lambda > 1$. In the diagrammatic notation,

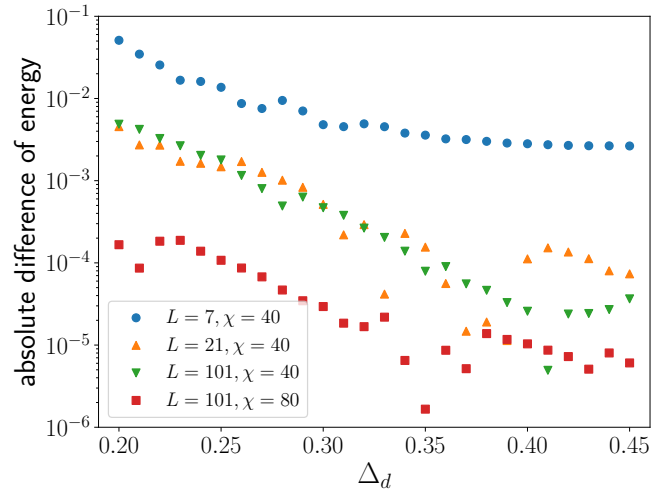


FIG. 3. Absolute difference of energy between those obtained from the correlation matrix of Gaussian fPEPS and direct tensor network contraction of an infinite fPEPS. The hole density is set to $\delta = 0.16$ and the virtual fermion flavor number in the Gaussian fPEPS is $\Lambda = 2$. χ is the bond dimension used in the variational uniform matrix product state algorithm [51]. This result reveals that for small system size, the difference mainly comes from the finite-size effect of Gaussian fPEPS and can be minimized by enlarging system size. If the system size is large enough, the difference comes from the finite bond dimension of environments in contraction. Nevertheless, the difference is quite small.

the two states differ by the corresponding swap gates

$$|\omega_{\mathbf{ij}}^C\rangle = \text{[Diagram showing a swap gate between two sites]} |\omega_{\mathbf{ij}}\rangle. \quad (16)$$

All these swap gates can be absorbed into the local tensor A_{uldr}^f . Afterwards, the tensor network state is compatible with the fPEPS convention in Ref. [49] and the resulting local tensor is suitable for a fPEPS tensor contraction code.

To compute expectation values, we consider an infinite fPEPS and adopt variational uniform matrix product state method [51] to contract infinite tensor networks. We note that other methods (e.g., corner transfer matrix renormalization group method [52, 53]) are also applicable.

III. RESULTS

The BCS Hamiltonian in Eq. (2) has Dirac points at $\mathbf{k} = (\pm\frac{\pi}{2}, \pm\frac{\pi}{2})$. When optimizing Γ , we choose a suitable combination of the system size L and boundary condition to avoid these exact zero modes, as we mentioned in Sec. II A.

First, as a sanity check, the expectation value of the Hamiltonian in Eq. (2) is calculated from optimized Gaussian fPEPS. The expectation value can be obtained in two different ways. The first way is through tensor network contraction, and the second way is using the correlation matrix [see Eq. (11)]. The result in Fig. 3 shows that the energy evaluated

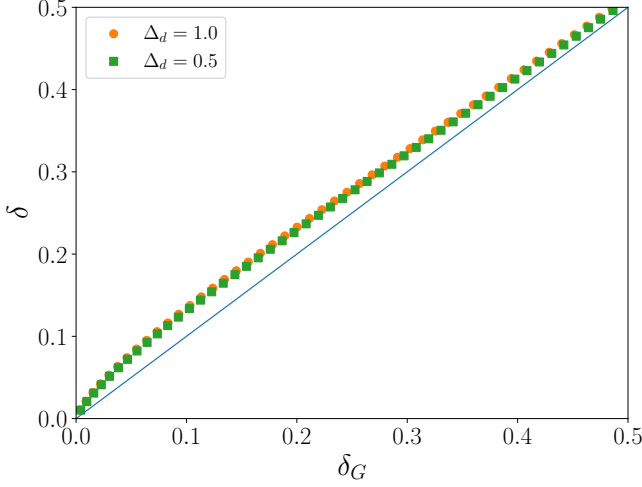


FIG. 4. Hole density before (δ) and after (δ_G) the Gutzwiller projection. Here, we consider $\Lambda = 2$ and $L = 101$. The deviation of points from the blue line represents the error of the Gutzwiller approximation for the hole fugacity in Eq. (14).

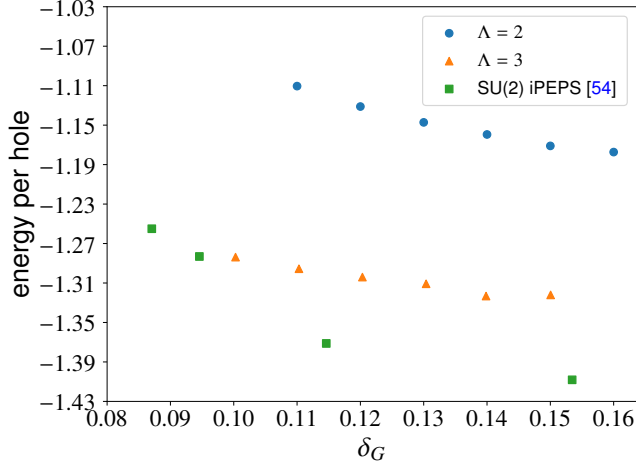


FIG. 5. Energy per hole. In $\Lambda = 2$ cases, we vary Δ_d to minimize the energy of the t - J model for a given density of holes δ_G . Fugacity in the Gutzwiller projector is tuned for each Δ_d to ensure the final δ_G be the same, which is crucial in finding optimized Δ_d . For $\Lambda = 3$ cases, we used optimized Δ_d and solved fugacity in $\Lambda = 2$ for each δ to avoid a costly optimization of Δ_d and solution of fugacity in $\Lambda = 3$. Green squares are from SU(2) fPEPS calculations in [54].

in these two ways agrees with each other. The small discrepancy is due to the finite bond dimension of environments in the tensor network contraction. Such discrepancy can be reduced systematically by enlarging the bond dimension kept in the contraction.

Next, we move on to the Gutzwiller projected states. We denote the density of holes of unprojected fPEPS as δ and that of Gutzwiller projected state as δ_G , respectively. With a suitable choice of hole fugacity z , we expect $\delta = \delta_G$. Here, we examine the Gutzwiller approximated fugacity $z = 2\delta/(1 + \delta)$ [46]. The result in Fig. 4 shows that the approx-

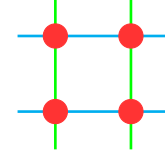


FIG. 6. The density of charge and pairing strength of the Gutzwiller projected BCS state in the case of $\Lambda = 2, \delta = 0.16, \Delta_d = 0.25$. The diameter of red circles scales with the quantity of density of holes. The width of cyan and green lines scales with the absolute value of pairing strength where the sign of the pairing strength is positive(negative) for the cyan(green) lines.

imated fugacity is smaller than needed since δ is larger than δ_G . Thus, the fugacity should be enlarged to make sure that δ remains unchanged after the Gutzwiller projection.

The projected d-wave pairing state is believed to be a good candidate for the ground state of the t - J model [4] with the Hamiltonian [55, 56]

$$H_{t,J} = -t \sum_{\langle i,j \rangle, \sigma} P_G (f_{i\sigma}^\dagger f_{j\sigma} + \text{h.c.}) P_G + J \sum_{\langle i,j \rangle} (\mathbf{S}_i \cdot \mathbf{S}_j - \frac{n_i n_j}{4}), \quad (17)$$

where $\mathbf{S}_i = \frac{1}{2} \sum_{ab} f_{i,a}^\dagger \boldsymbol{\sigma}_{ab} f_{i,b}$ and $n_i = \sum_{\sigma} f_{i\sigma}^\dagger f_{i\sigma}$ are spin and charge density operators, respectively. We set $J/t = 0.4$ ($t = 1$) and carry out a variational calculation for the Gutzwiller projected d-wave ansatz.

Treating Δ_d in Eq. (2) as the single variational parameter, we need to optimize the variational energy of $H_{t,J}$ (denoted as $E_{t,J}$) for each given hole concentration δ_G . In the calculation, it is crucial to keep the same δ_G when varying Δ_d since the variational energy is very sensitive to δ_G . We achieve this by tuning the fugacity using a bisection search as an inner loop for the variational optimization of Δ_d .

Figure 6 shows the measured correlations for an optimized state. The state is uniform and does not exhibit magnetic or charge order but hosts a d-wave superconducting order.

Directly observing a perfect dome shape in the order parameter $\frac{1}{\sqrt{2}} |\langle f_{i\uparrow} f_{j\downarrow} - f_{i\downarrow} f_{j\uparrow} \rangle|$ for the neighboring site \mathbf{i}, \mathbf{j} is difficult for some reasons. The convergence of the variational uniform matrix product state algorithm is difficult for small Δ_d and δ_G . Thus, the range of investigated δ_G is limited to (0.11, 0.16). Besides, the tensor network contraction error makes it difficult to find optimal Δ_d and corresponding order parameter with high precision. As an outlook, it might be possible to improve the convergence and precision by exploiting the SU(2) symmetry of the fPEPS in tensor network contractions [57].

As the bisection search of z is unaffordable for $\Lambda = 3$, we investigate the order parameter for $\Lambda = 2$. As shown in Fig. 7, in the limited range of δ_G , the optimal variational parameter Δ_d decreases with doping and the pairing order parameter increases with doping. On the other hand, the order parameter increases with Δ_d for a fix doping. Putting these three facts together, it can be expected that for larger δ_G , the order parameter will decrease as the optimal Δ_d decreases with doping and finally drop to zero. In conclusion, one would obtain a dome shape in the order parameter versus doping.

Lastly, we compute the energy per hole $(E_{t,J} + 0.46778)/\delta_G$

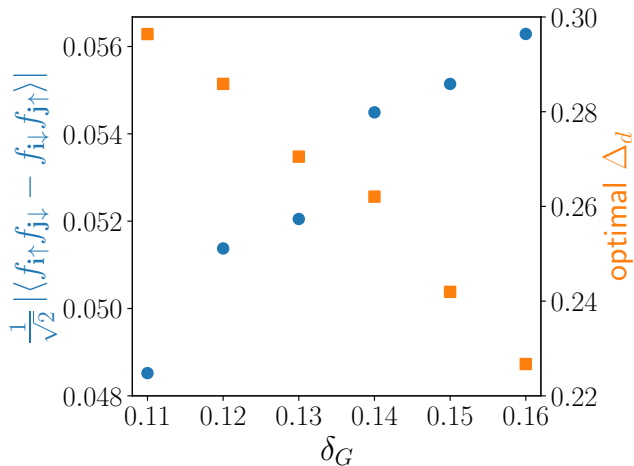


FIG. 7. Order parameter $\frac{1}{\sqrt{2}} |\langle f_{i\uparrow}f_{j\downarrow} - f_{i\downarrow}f_{j\uparrow} \rangle|$ (blue circle) for neighboring sites \mathbf{i}, \mathbf{j} and optimal Δ_d (orange square) versus δ_G for $\Lambda = 2$ and $L = 101$. The order parameter is obtained by using the tensor network contraction. For stability, the optimal Δ_d is determined via a second degree polynomial fitting near the optimal points.

for $\Lambda = 2$ and 3 where -0.46778 is the ground-state energy for the undoped case [58]. Increasing bond dimension results in a low energy expectation value, reaching an energy per hole as low as -1.32 . The energies are higher than those obtained from direct optimization of fPEPS in Refs. [17, 54]. Figure 5 shows the energy per hole as a function of doping. We compare the energy with the SU(2) fPEPS results of Ref. [54] obtained at $D^* = 6$, which amounts to $D \approx 11$ without symmetry. Note that for $\Lambda = 3$, our fPEPS obtained from the Gutzwiller ansatz has bond dimension $D = 8$. Besides, our fPEPS tensor is uniform, while Ref. [54] uses a 2×2 or 5×2 unit cell. Constructing a tensor network representation of projected d-wave pairing states opens the way to provide good initial states in variational calculations besides offering diagnosis from the tensor network toolbox.

IV. SUMMARY AND DISCUSSIONS

To summarize, we have developed a systematic method to construct the fPEPS representation of projected BCS states. Using the method, we investigated the physical properties of the projected d-wave pairing state on an infinite square lattice. In particular, the estimated variational energy for the t - J model is comparable to the results from tensor network optimizations. The code implementation is available online [59].

Our approach can also be applied to other classes of projected fermionic states, such as those obtained from Chern insulators and spin density wave states [60]. In certain cases, one would need an enlarged unit cell in the construction and contraction of the tensor networks. In contrast to previous works [35, 36, 61–64] which rely on an analytical PEPS representation of the RVB state, the present approach variationally solves a fermionic quadratic Hamiltonian of unprojected states using Gaussian fPEPS [42]. Thus, the present approach has a broader range of applications and can be systematically improved by increasing the bond dimension of the Gaussian fPEPS tensor.

Partial Gutzwiller projection which suppresses but does not eliminate double occupancies [65] can also be straightforwardly implemented. These states are relevant to the study of Gossamer superconductors [66, 67] and Hubbard models. In principle, long-range Jastrow factors beyond the onsite Gutzwiller projection can be applied by using its tensor network form [68]. This class of states is considered to be crucial for describing Mott transitions [69]. Further investigations of these states with our method are left for future works.

V. ACKNOWLEDGMENTS

We thank Jan von Delft, Jheng-Wei Li, and Yi Zhou for useful discussions. This project is supported by the Strategic Priority Research Program of the Chinese Academy of Sciences under Grant No. XDB30000000, the National Natural Science Foundation of China under Grant No. T2121001, and the Deutsche Forschungsgemeinschaft (DFG) through project A06 of SFB 1143 (project-id 247310070).

-
- [1] P. A. Lee, *Rep. Prog. Phys.* **71**, 012501 (2007).
 - [2] P. W. Anderson, *Science* **235**, 1196 (1987).
 - [3] G. Baskaran and P. W. Anderson, *Phys. Rev. B* **37**, 580 (1988).
 - [4] P. W. Anderson, P. A. Lee, M. Randeria, T. M. Rice, N. Trivedi, and F. C. Zhang, *J. Phys. Condens. Matter* **16**, R755 (2004).
 - [5] P. Fazekas and P. W. Anderson, *Philos. Mag.* **30**, 423 (1974).
 - [6] F. C. Zhang, C. Gros, T. M. Rice, and H. Shiba, *Supercond. Sci. Technol.* **1**, 36 (1988).
 - [7] C. Gros, *Phys. Rev. B* **38**, 931 (1988).
 - [8] C. Gros, *Ann. Phys.* **189**, 53 (1989).
 - [9] H. Yokoyama and H. Shiba, *J. Phys. Soc. Jpn.* **57**, 2482 (1988).
 - [10] A. Paramekanti, M. Randeria, and N. Trivedi, *Phys. Rev. Lett.* **87**, 217002 (2001).
 - [11] B. Edegger, V. N. Muthukumar, and C. Gros, *Adv. Phys.* **56**, 927 (2007).
 - [12] H. Yokoyama and M. Ogata, *J. Phys. Soc. Jpn.* **65**, 3615 (1996).
 - [13] D. A. Ivanov, *Phys. Rev. B* **70**, 104503 (2004).
 - [14] M. Lugas, L. Spanu, F. Becca, and S. Sorella, *Phys. Rev. B* **74**, 165122 (2006).
 - [15] A. S. Darmawan, Y. Nomura, Y. Yamaji, and M. Imada, *Phys. Rev. B* **98**, 205132 (2018).
 - [16] T. Misawa, S. Morita, K. Yoshimi, M. Kawamura, Y. Motoyama, K. Ido, T. Ohgoe, M. Imada, and T. Kato, *Comput. Phys. Commun.* **235**, 447 (2019).
 - [17] P. Corboz, T. M. Rice, and M. Troyer, *Phys. Rev. Lett.* **113**, 046402 (2014).

- [18] B. X. Zheng, C. M. Chung, P. Corboz, G. Ehlers, M. P. Qin, R. M. Noack, H. Shi, S. R. White, S. Zhang, and G. K. L. Chan, *Science* **358**, 1155 (2017).
- [19] B. Ponsioen, S. S. Chung, and P. Corboz, *Phys. Rev. B* **100**, 195141 (2019).
- [20] H.-C. Jiang and S. A. Kivelson, *Phys. Rev. Lett.* **127**, 097002 (2021).
- [21] S. Gong, W. Zhu, and D. N. Sheng, *Phys. Rev. Lett.* **127**, 097003 (2021).
- [22] S. Jiang, D. J. Scalapino, and S. R. White, *Proc. Natl. Acad. Sci.* **118**, e2109978118 (2021).
- [23] M. Qin, C.-M. Chung, H. Shi, E. Vitali, C. Hubig, U. Schollwöck, S. R. White, and S. Zhang (Simons Collaboration on the Many-Electron Problem), *Phys. Rev. X* **10**, 031016 (2020).
- [24] S. Sorella, (2021), [arXiv:2101.07045](https://arxiv.org/abs/2101.07045).
- [25] P. Silvi, D. Rossini, R. Fazio, G. E. Santoro, and V. Giovannetti, *Int. J. Mod. Phys. B* **27**, 1 (2013).
- [26] M. P. Zaletel, *Exact tensor network ansatz for strongly interacting systems*, Ph.D. thesis, UC Berkeley (2014).
- [27] M. T. Fishman and S. R. White, *Phys. Rev. B* **92**, 075132 (2015).
- [28] B. Bauer, B. P. Keller, S. Trebst, and A. W. W. Ludwig, *Phys. Rev. B* **99**, 035155 (2019).
- [29] Y.-H. Wu, L. Wang, and H.-H. Tu, *Phys. Rev. Lett.* **124**, 246401 (2020).
- [30] H.-K. Jin, H.-H. Tu, and Y. Zhou, *Phys. Rev. B* **101**, 165135 (2020).
- [31] G. Petrica, B.-X. Zheng, G. K.-L. Chan, and B. K. Clark, *Phys. Rev. B* **103**, 125161 (2021).
- [32] H.-K. Jin, H.-H. Tu, and Y. Zhou, *Phys. Rev. B* **104**, L020409 (2021).
- [33] A. M. Aghaei, B. Bauer, K. Shtengel, and R. V. Mishmash, (2020), [arXiv:2009.12435](https://arxiv.org/abs/2009.12435).
- [34] H.-K. Jin, R.-Y. Sun, Y. Zhou, and H.-H. Tu, *Phys. Rev. B* **105**, L081101 (2022).
- [35] F. Verstraete, M. M. Wolf, D. Perez-Garcia, and J. I. Cirac, *Phys. Rev. Lett.* **96**, 220601 (2006).
- [36] D. Poilblanc, N. Schuch, D. Pérez-García, and J. I. Cirac, *Phys. Rev. B* **86**, 014404 (2012).
- [37] D. Poilblanc, P. Corboz, N. Schuch, and J. I. Cirac, *Phys. Rev. B* **89**, 241106 (2014).
- [38] C. V. Kraus, N. Schuch, F. Verstraete, and J. I. Cirac, *Phys. Rev. A* **81**, 052338 (2010).
- [39] T. B. Wahl, S. T. Haßler, H.-H. Tu, J. I. Cirac, and N. Schuch, *Phys. Rev. B* **90**, 115133 (2014).
- [40] S. Bravyi, *Quantum Inf. and Comp.* **5**, 216 (2005).
- [41] Together with suitably chosen system sizes, this boundary condition avoids the complication of dealing with exact zero modes at the Dirac points $\mathbf{k} = (\pm\frac{\pi}{2}, \pm\frac{\pi}{2})$ of the d-wave pairing Hamiltonian.
- [42] Q. Mortier, N. Schuch, F. Verstraete, and J. Haegeman, (2020), [arXiv:2008.11176](https://arxiv.org/abs/2008.11176).
- [43] J. Bradbury, R. Frostig, P. Hawkins, M. J. Johnson, C. Leary, D. Maclaurin, G. Necula, A. Paszke, J. VanderPlas, S. Wanderman-Milne, and Q. Zhang, “JAX: composable transformations of Python+NumPy programs,” (2018).
- [44] J. Townsend, N. Koep, and S. Weichwald, *J. Mach. Learn. Res.* **17**, 1 (2016).
- [45] B. A. Bernevig, R. B. Laughlin, and D. I. Santiago, *Phys. Rev. Lett.* **91**, 147003 (2003).
- [46] B. Edegger, N. Fukushima, C. Gros, and V. N. Muthukumar, *Phys. Rev. B* **72**, 134504 (2005).
- [47] P. Anderson and N. Ong, *J. Phys. Chem. Solids* **67**, 1 (2006).
- [48] C.-P. Chou, F. Yang, and T.-K. Lee, *Phys. Rev. B* **85**, 054510 (2012).
- [49] P. Corboz, R. Orús, B. Bauer, and G. Vidal, *Phys. Rev. B* **81**, 165104 (2010).
- [50] P. Corboz and G. Vidal, *Phys. Rev. B* **80**, 165129 (2009).
- [51] V. Zauner-Stauber, L. Vanderstraeten, M. T. Fishman, F. Verstraete, and J. Haegeman, *Phys. Rev. B* **97**, 045145 (2018).
- [52] T. Nishino and K. Okunishi, *J. Phys. Soc. Jpn.* **66**, 3040 (1997).
- [53] R. Orús and G. Vidal, *Phys. Rev. B* **80**, 094403 (2009).
- [54] J.-W. Li, B. Bruognolo, A. Weichselbaum, and J. von Delft, *Phys. Rev. B* **103**, 075127 (2021).
- [55] F. C. Zhang and T. M. Rice, *Phys. Rev. B* **37**, 3759 (1988).
- [56] M. Ogata and H. Fukuyama, *Rep. Prog. Phys.* **71**, 036501 (2008).
- [57] H.-H. T. Jheng-Wei Li, Jan von Delft, [arXiv:2208.xxxxx](https://arxiv.org/abs/2208.xxxxx).
- [58] A. W. Sandvik, *Phys. Rev. B* **56**, 11678 (1997).
- [59] <https://github.com/TensorBFS/Gaussian-fPEPS>.
- [60] I. Affleck and J. B. Marston, *Phys. Rev. B* **37**, 3774 (1988).
- [61] N. Schuch, D. Poilblanc, J. I. Cirac, and D. Pérez-García, *Phys. Rev. B* **86**, 115108 (2012).
- [62] L. Wang, D. Poilblanc, Z.-C. Gu, X.-G. Wen, and F. Verstraete, *Phys. Rev. Lett.* **111**, 037202 (2013).
- [63] D. Poilblanc, P. Corboz, N. Schuch, and J. I. Cirac, *Phys. Rev. B* **89**, 241106 (2014).
- [64] S. Yang, T. B. Wahl, H.-H. Tu, N. Schuch, and J. I. Cirac, *Phys. Rev. Lett.* **114**, 106803 (2015).
- [65] M. C. Gutzwiller, *Phys. Rev. Lett.* **10**, 159 (1963).
- [66] R. B. Laughlin, *Philos. Mag.* **86**, 1165 (2006).
- [67] F. C. Zhang, *Phys. Rev. Lett.* **90**, 207002 (2003).
- [68] Z. Li, M. J. O’Rourke, and G. K.-L. Chan, *Phys. Rev. B* **100**, 155121 (2019).
- [69] M. Capello, F. Becca, M. Fabrizio, S. Sorella, and E. Tosatti, *Phys. Rev. Lett.* **94**, 026406 (2005).
- [70] Rigorously speaking, composite Hilbert space $\mathcal{H}_1 \otimes \mathcal{H}_2$ of fermions should be viewed as a \mathbb{Z}_2 -graded tensor product rather than a usual tensor product. However, this distinction is unnecessary for our purpose here, as the operators under consideration are density operators involving even Majorana modes.
- [71] A. Hackenbroich, B. A. Bernevig, N. Schuch, and N. Regnault, *Phys. Rev. B* **101**, 115134 (2020).
- [72] T. B. Wahl, H.-H. Tu, N. Schuch, and J. I. Cirac, *Phys. Rev. Lett.* **111**, 236805 (2013).
- [73] G. F. Bertsch and L. M. Robledo, *Phys. Rev. Lett.* **108**, 042505 (2012).
- [74] C. Bloch and A. Messiah, *Nucl. Phys.* **39**, 95 (1962).
- [75] M. Wimmer, *ACM Trans. Math. Softw.* **38** (2012).
- [76] S. Morita, R. Kaneko, and M. Imada, *J. Phys. Soc. Jpn.* **84**, 024720 (2015).
- [77] S. R. White, *Phys. Rev. Lett.* **69**, 2863 (1992).

Appendix A: Proof of Eq. (10)

To establish the relationship between the correlation matrix of the Gaussian fPEPS and that of the fiducial state in Eq. (6), we prove a general result below.

Let us consider a fermionic Gaussian state $|\omega\rangle$ living in the Hilbert space \mathcal{H}_2 with virtual Majorana modes d_l ($l = 1, \dots, 2m$) and another fermionic Gaussian state $|A\rangle$ living in the composite Hilbert space $\mathcal{H}_1 \otimes \mathcal{H}_2$ including both physical and virtual Majorana modes [70], where the physical modes are denoted as c_j ($j = 1, \dots, 2n$).

The overlap $\langle \omega|A \rangle$ is also a fermionic Gaussian state and lives in the physical Hilbert space \mathcal{H}_1 . To calculate its correlation matrix, it is convenient to work with the density operators and write the density operator associated with $\langle \omega|A \rangle$ as

$$\rho_f(c) = \langle \omega|A \rangle \langle A|\omega \rangle = \text{tr}_d[\rho_A(c, d)\rho_\omega(d)], \quad (\text{A1})$$

where tr_d is the partial trace of d -modes and ρ_ω (ρ_A) is the density operator of $|\omega \rangle$ ($|A \rangle$).

We shall establish a Grassmann integration approach to calculate the partial trace in Eq. (A1). This approach uses the Grassmann representations of the Gaussian density operators ρ_ω and ρ_A [40],

$$g_\omega(\tau) = \frac{1}{2^m} \exp\left(\frac{i}{2}\tau^T \Gamma_\omega \tau\right), \quad (\text{A2})$$

and

$$g_A(\theta, \zeta) = \frac{1}{2^{n+m}} \exp\left[\frac{i}{2} \begin{pmatrix} \theta^T & \zeta^T \\ -B^T & D \end{pmatrix} \begin{pmatrix} A & B \\ -B^T & D \end{pmatrix} \begin{pmatrix} \theta \\ \zeta \end{pmatrix}\right], \quad (\text{A3})$$

where $\theta = (\theta_1, \dots, \theta_{2n})^T$ is a vector of real Grassmann variables for the physical modes $c = (c_1, \dots, c_{2n})^T$ and, similarly, τ and ζ include Grassmann variables for virtual modes. Here Γ_ω and $\begin{pmatrix} A & B \\ -B^T & D \end{pmatrix}$ are the correlation matrices of ρ_ω and ρ_A , respectively.

In the Grassmann representation, the partial trace of virtual modes in Eq. (A1) can be calculated using a Grassmann integration as follows:

$$g_f(\theta) = (-2)^m \int D\zeta D\tau e^{\zeta^T \tau} g_A(\theta, \zeta) g_\omega(\tau), \quad (\text{A4})$$

where $g_f(\theta)$ is the Grassmann representation of the (unnormalized) density operator for $\langle \omega|A \rangle$ and the integration is over Grassmann variables associated with virtual modes, with the notation $\int D\zeta D\tau = \int d\zeta_{2m} \dots d\zeta_1 d\tau_{2m} \dots d\tau_1$. The proof of (A4) is done by comparing the outcomes of Eqs. (A1) and (A4), where the former can be computed by expanding ρ_A and ρ_ω in terms of Majorana operators and performing the partial trace, and the latter is computed by expanding the Grassmann exponential and carrying out the integration over Grassmann variables one by one.

After substituting Eqs. (A2) and (A3) into Eq. (A4) and performing the Gaussian integration over ζ and τ , we obtain

$$g_f(\theta) = \frac{1}{2^{n+m}} \text{Pf}(\Gamma_\omega) \text{Pf}(D - \Gamma_\omega^{-1}) \exp\left(\frac{i}{2}\theta^T \Gamma_f \theta\right), \quad (\text{A5})$$

where Γ_f is the correlation matrix of $\langle \omega|A \rangle$ and has the following explicit form:

$$\begin{aligned} \Gamma_f &= A + B(D - \Gamma_\omega^{-1})^{-1} B^T \\ &= A + B(D + \Gamma_\omega)^{-1} B^T. \end{aligned} \quad (\text{A6})$$

Here we used $\Gamma_\omega^{-1} = -\Gamma_\omega$ as $|\omega \rangle$ is a pure state.

We note that Eq. (10) is just the Fourier transformed version of (A6) taking into account the translation invariance. It

is also worth mentioning that Eq. (A6) agrees with Eq. (C8) in Ref. [71] but differs from those in Refs. [38, 39, 72] by the sign in front of Γ_ω . The reason of this difference is that the Gaussian fPEPS projectors in Refs. [38, 39, 72] are defined through Gaussian maps, whose action is not exactly equivalent to the overlap form in Eq. (3).

Appendix B: Overlap-based translation

Instead of diagonalizing the fiducial Hamiltonian in the Fock space, we provide below an alternative approach to obtain the explicit tensor form of $|A_i \rangle$. This approach is based on an overlap formula between fermionic Gaussian states and Fock states.

To start with, we rewrite the fiducial Hamiltonian (13) in a Bogoliubov-de Gennes (BdG) form by converting the Majorana operators γ back to original complex fermions

$$H = \begin{pmatrix} c^\dagger & c \end{pmatrix} \mathcal{H} \begin{pmatrix} c \\ c^\dagger \end{pmatrix}, \quad (\text{B1})$$

where $(c^\dagger \ c)$ is a row vector of fermionic creation and annihilation operators for $4\Lambda + 2$ physical and virtual fermions at a local site (see Sec. II A). The BdG single-particle Hamiltonian \mathcal{H} is diagonalized by a Bogoliubov transformation

$$\begin{pmatrix} a^\dagger & a \end{pmatrix} = \begin{pmatrix} c^\dagger & c \end{pmatrix} \begin{pmatrix} U & V^* \\ V & U^* \end{pmatrix}, \quad (\text{B2})$$

where $(a^\dagger \ a)$ includes creation and annihilation operators of Bogoliubov modes and the Bogoliubov matrices U and V satisfy

$$U^\dagger U + V^\dagger V = \mathbb{I}, \quad U^T V + V^T U = \mathbb{O} \quad (\text{B3})$$

with \mathbb{I} (\mathbb{O}) being the identity (zero) matrix.

The local fiducial state $|A_i \rangle$, as the ground state of H , is annihilated by all a -fermion annihilation operators. According to Eq. (5), the tensor form of $|A_i \rangle$ can be obtained by calculating each coefficient A_{uldr}^f which is the overlap $\langle f| \otimes \langle uldr|A_i \rangle$. $\langle f| \otimes \langle uldr|$ denotes a Fock state in the c -fermion basis and can generally be written as ${}_c \langle 0|c_{i_{M'}} \dots c_{i_1}$ with $0 \leq M' \leq 4\Lambda + 2$ and $1 \leq i_1 < \dots < i_{M'} \leq 4\Lambda + 2$, where ${}_c \langle 0|$ is the c -fermion vacuum.

Such overlap calculation can be carried out by rewriting the Bogoliubov vacuum $|A_i \rangle$ in a suitable form [73], with the help of the Bloch-Messiah decomposition [74]

$$\begin{pmatrix} U & V^* \\ V & U^* \end{pmatrix} = \begin{pmatrix} D & 0 \\ 0 & D^* \end{pmatrix} \begin{pmatrix} \bar{U} & \bar{V} \\ \bar{V} & \bar{U} \end{pmatrix} \begin{pmatrix} C & 0 \\ 0 & C^* \end{pmatrix}, \quad (\text{B4})$$

where D and C are unitary matrices and \bar{U} and \bar{V} are real matrices with the following form:

$$\bar{U} = \begin{pmatrix} \mathbb{O} & & \\ & \bigoplus_p u_p \sigma^0 & \\ & & \mathbb{I} \end{pmatrix}, \quad \bar{V} = \begin{pmatrix} \mathbb{I} & & \\ & \bigoplus_p iv_p \sigma^y & \\ & & \mathbb{O} \end{pmatrix}. \quad (\text{B5})$$

Here u_p and v_p are positive and satisfy $u_p^2 + v_p^2 = 1$, \mathbb{I} (\mathbb{O}) is the identity (zero) matrix, σ^0 and σ^y are the 2×2 identity and Pauli matrices. For our purpose, it is convenient to truncate the \mathbb{I} (\mathbb{O}) block in \bar{U} (\bar{V}) to obtain matrices

$$\bar{U}' = \begin{pmatrix} \mathbb{O} \\ \bigoplus_p u_p \sigma^0 \end{pmatrix}_{M \times M}, \quad \bar{V}' = \begin{pmatrix} \mathbb{I} \\ \bigoplus_p i v_p \sigma^y \end{pmatrix}_{M \times M}. \quad (\text{B6})$$

Following Ref. [34], $|A_i\rangle$ is represented as

$$|A_i\rangle = \frac{1}{\prod_p v_p} b_1 \cdots b_M |0\rangle_c, \quad (\text{B7})$$

where $b = c^\dagger D' \bar{V}' + c(D')^* \bar{U}'$. Here D' is a $(4\Lambda + 2) \times M$ matrix obtained by keeping the first M columns of the unitary matrix D [see Eq. (B4)], which is an isometry satisfying $(D')^\dagger D' = \mathbb{I}_{M \times M}$.

With these results in hand, the tensor entry A_{uldr}^f is calculated with Wick's theorem as follows:

$$\begin{aligned} \langle f | \otimes \langle uldr | A_i \rangle &= \frac{1}{\prod_p v_p} {}_c \langle 0 | c_{i_{M'}} \cdots c_{i_1} b_1 \cdots b_M | 0 \rangle_c \\ &= \frac{(-1)^{\frac{1}{2} M' (M' - 1)}}{\prod_p v_p} {}_c \langle 0 | c_{i_1} \cdots c_{i_{M'}} b_1 \cdots b_M | 0 \rangle_c \\ &= \frac{(-1)^{\frac{1}{2} M' (M' - 1)}}{\prod_p v_p} \text{Pf} \begin{pmatrix} \mathbb{O}_{M' \times M'} & \mathbb{R}_{M' \times M} \\ -\mathbb{R}_{M \times M'}^T & \mathbb{Q}_{M \times M} \end{pmatrix}, \quad (\text{B8}) \end{aligned}$$

where $\mathbb{R}_{m'm} = {}_c \langle 0 | c_{i_{m'}} b_m | 0 \rangle_c = (D' \bar{V}')_{i_{m'} m}$ and $\mathbb{Q}_{m'm} = {}_c \langle 0 | b_{m'} b_m | 0 \rangle_c = (\bar{U}' \bar{V}')_{m' m}$. Note, however, that the overlap in Eq. (B8) vanishes if M and M' have different parity (this automatically encodes the fermion parity symmetry). The pfaffian formula (B8) allows us to calculate the explicit tensor form of $|A_i\rangle$. In our program, the pfaffian is calculated with an algorithm provided by M. Wimmer [75].

We can compare the pros and cons of Hamiltonian-based translation and overlap-based translation: The complexity of translation is quantified by $N = 4\Lambda + 2$. When employing an overlap-based algorithm, we need to calculate matrix pfaffians for 2^{N-1} times. As the size of each matrix is of order $2N \times 2N$, the computational cost of the overlap-based translation is $O(N^3 \times 2^{N-1})$. This complexity can be further reduced to $O(N^2 \times 2^{N-1})$ if a fast update technique for pfaffian is used (see, e.g., Ref. [76]). Meanwhile, in the Hamiltonian-based algorithm, the computational cost of obtaining the dominant eigenvector of a $2^N \times 2^N$ matrix scales as $O((2^N)^2) = O(2^{2N})$.

When Λ is large, the Hamiltonian-based algorithm in Sec. II C has a larger computational cost, but it is nevertheless more straightforward and intuitive. If Λ is so large that an exact diagonalization of the fiducial Hamiltonian is not feasible, one might also employ the density matrix renormalization group method [77] to obtain an approximation of $|A_i\rangle$.